Results in Physics 23 (2021) 104078

Contents lists available at ScienceDirect

Results in Physics

journal homepage: www.elsevier.com/locate/rinp

A high order multi-resolution WENO numerical scheme for solving viscous quantum hydrodynamic model for semiconductor devices

Tauqeer Ahmed [a,*], Asad Rehman [b], Ashiq Ali [a], Shamsul Qamar [a,c]

[a] Department of Mathematics, COMSATS University Islamabad, Park Road Chak Shahzad, 45550, Islamabad, Pakistan
[b] Department of Mathematics, University of Education, Johar Town, , 54770, Lahore, Pakistan
[c] Max Planck Institute for Dynamics of Complex Technical Systems, Sandtorstrasse 1, 39106 Magdeburg, Germany

ARTICLE INFO

Keywords:
Viscous quantum hydrodynamic
Semiconductor devices
Current density
Multi-resolution
WENO scheme

ABSTRACT

In this article, fifth order finite volume multi-resolution weighted essentially non-oscillatory (MR-WENO) scheme is developed for solving one-dimensional non linear viscous quantum hydrodynamical model for semiconductor devices with constant temperature. This non linear model consists of three equations, two equations for the current density and electron density, and third equation is the Poisson equation. The first two equations include the viscous and quantum correction terms. Further, numerical technique is used to obtain the solution due to high non linearity of considered model. The multi-resolution technique is used to reduce the computational cost of high resolution numerical scheme. In the procedure of derivation of the MR-WENO scheme unequal central spatial stencils are used and linear weights can be chosen any positive numbers with only restriction that their total sum is one. Various numerical test problems are considered to check the validity and accuracy of the derived numerical scheme. Further, the results obtained from considered numerical scheme are compared with those of kinetic flux vector splitting numerical scheme.

Introduction

Modeling and numerical simulation of semiconductor processes are essential to increase the efficiency of new quantum devices and equally important to reduce manufacturing cost and time. Quantum semiconductor devices are playing an increasingly important role in advanced micro-electronic applications, including multiple-state logic and memory devices [1–4]. To model such type of devices, the classical hydrodynamic model for semiconductor devices was extended to include $0(h^2)$ quantum corrections [5]. In simulation of the semiconductor devices, the small sizes (0.1 micro meter) of the characteristics devices length make the modeling of quantum effects more important and these effects are included by using the microscopic equations such as Schrodinger or Wigner equations [6,7]. Initially, the kinetic Wigner equation [6,7] is used to model the quantum semiconductor devices. But in this equation the Wigner distribution function depends on various parameters such as, wave vector, space and time, therefore numerical simulation of such equation is computationally expensive. So in recent years, macroscopic quantum equations are presented and used for simulations of quantum devices, for further detail, the reader is referred to [8–13]. This presentation of quantum equations has various advantages such that, these equations are computationally less expensive, can be described in the macroscopic quantities like current density and particle density, and the macroscopic boundary conditions can be introduced [14]. By keeping all these advantages in mind, here we have numerically investigated the viscous quantum hydrodynamical model (VQHDM) that is derived from Wigner–Fokker–Planck equations. For extensive detail about derivation of the proposed model, the reader is referred to [14,15].

Due to the importance of viscous quantum hydrodynamical model for semiconductor devices, many researchers have paid special attention to analyze theoretically and numerically these types of models, for detail see [14,16–21]. In the article [14], the viscous quantum hydrodynamic model was approximated by two different numerical schemes namely central finite difference and relaxation schemes. The authors show that central finite difference scheme is more appropriate to compute the model numerically as compare to the relaxation scheme since the presence of numerical viscosity in the relaxtion scheme changes the nature of the numerical solutions. Subsequently, the authors used the kinetic flux vector splitting (KFVS) scheme to numerically investigate the viscous quantum hydrodynamic model [21].

In this article, fifth order finite volume multi-resolution WENO scheme is developed to simulate the flow of electrons in semiconductor devices based on the viscous quantum hydrodynamic model. We borrow the idea of MR-WENO scheme from [22]. Just like the

* Corresponding author.
E-mail addresses: tauqeer968@gmail.com, SP16-PMT-008@ISBSTUDENT.COMSATS.EDU.PK (T. Ahmed).

https://doi.org/10.1016/j.rinp.2021.104078
Received 4 September 2020; Received in revised form 26 February 2021; Accepted 11 March 2021
Available online 18 March 2021

classical finite volume WENO schemes [23,24], the proposed numerical scheme also resolves the sharp discontinuities efficiently and ensures high order accuracy in the smooth regions, but the proposed numerical scheme uses the series of unequal sized hierarchical central spatial stencils, for further detail the reader is referred to the articles [22] and references therein. Basically, the multi-resolution techniques [25,26] were designed to reduce the computational costs of high resolution numerical algorithms. Since these multi-resolution schemes concentrate the regions of computational domain which include sharp gradients.

The organization of remaining article is as follow. In 'Viscous quantum hydrodynamic Model', the mathematical form of viscous quantum hydrodynamic model for semiconductor devices is explained. Next in 'Scaling of parameters', the scaling of proposed model is given and then compact form of the proposed model and boundary conditions are presented. In 'The multi-resolution WENO scheme for viscous quantum hydrodynamic model', the multi-resolution finite volume WENO numerical scheme is derived for the considered model. Subsequently, in 'Numerical test problems', the numerical solutions obtained from the considered numerical methods are compared with the results of the kinetic flux vector splitting numerical scheme [21] and with results are presented in [14]. Finally, in the section 'Conclusions', the conclusions are presented.

Viscous quantum hydrodynamic model

In this section, mathematical form of viscous quantum hydrodynamic model is explained. The current and electron density satisfy Madelung equations when the Schrodinger equations in a single state is separated into complex and real components.

$$\partial_t n + \frac{1}{q}\nabla.J = 0, \tag{1}$$

$$\partial_t J + \frac{1}{q}\nabla.\left(\frac{J\otimes J}{n}\right) - \frac{q^2}{m}n\nabla V - \frac{h^2 q}{6m^2}n\nabla\left(\frac{\triangle\sqrt{n}}{\sqrt{n}}\right) = 0, \tag{2}$$

here, spatial derivatives are represented by ∇ and $J\otimes J$ represents tensor whose components are $J_i J_k$ for $1 \le i \le d$ also $1 \le k \le d$ and d is the number of dimension. The other symbols of well known quantum hydrodynamic model are defined as: n—electron density, J—current density, q—elementary charge, m—effective electron mass, V—voltage and h—reduced Planck constant. In the article [27], the author has also expressed the above model as pressure-less Euler equations. The quantum hydrodynamic models (QHDM) have no impurities of the semiconductors such as electron's collision. For all intents and purposes these investigations of quantum hypothesis are in starting stages, for detail see [9,11,28]. The Wigner equation with the help of Fokker–Planck-type collision operator [29–31] can be re-written as

$$\partial_t w + \frac{h}{m}k\nabla_x w + \frac{q}{h}\Theta[V](w) = \frac{D_{pp}}{h^2}\triangle_k w + \frac{1}{\tau_0}\nabla_k(kw) + \frac{D_{pq}}{h}\nabla_x.\left(\nabla_k w\right) + D_{qq}\triangle_x w, \tag{3}$$

with

$$D_{pp} = \frac{mk_bT_0}{\tau_0},\quad D_{pq} = \frac{\Omega h^2}{6\pi k_bT_0\tau_0},\quad D_{qq} = \frac{h^2}{12mk_bT_0\tau_0},$$

here, the cut-off frequency is represented by Ω and the momentum relaxation time of the reservoir oscillators are represented by τ_0. The phase-space diffusion matrix is established by the constant terms D_{qq}, D_{pp} and D_{pq}. and fraction term is represented by $\frac{\nabla_k(kw)}{\tau_0}$ as discussed in [14]. By using Wigner–Fokker–Planck Eq. (3), the viscous quantum hydrodynamics model for semiconductor devices can be derived [15] as follows

$$\partial_t n + \frac{1}{q}\nabla.J = D_{qq}\triangle n, \tag{4}$$

$$\partial_t J + \frac{1}{q}\nabla.\left(\frac{J\otimes J}{n}\right) + \frac{qk_bT_0}{m}\left(1+\frac{D_{pq}}{k_bT_0}\right)\triangle n - \frac{q^2}{m}n\nabla V - \frac{h^2 q}{6m^2}n\nabla\left(\frac{\triangle\sqrt{n}}{\sqrt{n}}\right) = -\frac{J}{\tau_0} + D_{qq}\triangle J, \tag{5}$$

with Poisson equation

$$div_x(\varepsilon_s\nabla_x V) = q(n - C(x)), x \in \mathbb{R}^d \tag{6}$$

here, the permittivity of semiconductor is represented by ε_s, charge is represented by q and C is used for doping density profile. We treated $D_{pp}\triangle n$ and $D_{qq}\triangle J$ as viscous terms of order two.

Scaling of parameters

We introduce the characteristic length L (i.e device diameter) for scaling the VQHD Eq. (4) to (6) and all other quantities are defined as $C^* = \sup|C|$ is the characteristics density , $J^* = \frac{C^* t^* q k_B T_0}{Lm}$ is the current density and $V^* = \frac{k_B T_0}{q}$ is the voltage and the mean free-path l is given as $l^2 = \frac{k_b T_0 \tau_0^2}{m}$. We will get the value of t^* from the relation $L^2 = \frac{(t^*)^2 k_B T_0}{m}$. The dimensionless parameters are given as

$$x = \frac{x}{L},\ t = \frac{t}{t^*},\ C = \frac{C}{C^*},\ n = \frac{n}{C^*},\ J = \frac{J}{J^*},\ V = \frac{V}{V^*},$$

$$\tau = \frac{\tau_0}{t^*},\ \upsilon = \frac{t^*}{6\tau_0}\left(\frac{L_b}{L}\right)^2,\ \epsilon^2 = \frac{2}{3}\left(\frac{L_b}{L}\right)^2,\ \lambda^2 = \frac{\epsilon_s k_B T_0}{q^2 L^2 C*},$$

$$T = 1 + \frac{\Omega L_b h}{\sqrt{18}\pi k_B T_0 l},$$

here, the constant value $L_b = \frac{h}{\sqrt{2k_B m T_0}}$ is called de Broglie length. The scaled VQHDM is written by:

$$\partial_t n + \nabla.J = \upsilon\triangle n, \tag{7}$$

$$\partial_t J + \nabla.\left(\frac{J\otimes J}{n}\right) - n\nabla\left(V + V_{ext}\right) + T\nabla n - \frac{\epsilon^2}{2}n\nabla\left(\frac{\triangle\sqrt{n}}{\sqrt{n}}\right) = -\frac{J}{\tau} + \upsilon\triangle J, \tag{8}$$

$$\lambda^2\triangle V = (n - C) \tag{9}$$

where, the viscosity constant υ is positive. The heterogeneous semiconductor materials are modeled by the external potential $V_{ext}(x)$ introduced in Eq. (8). The value $C^* = 10^{24}$ m^3 is assumed to consider doping in m^3 The values of parameters obtained after scaling are given as $\lambda^2 = 3.032\times10^{-4}$, $\epsilon^2 = 3.893\times10^{-3}$, $T = 1.00585$ and $\upsilon = 9.935\times10^{-4}$.

Compact form of the model

The compact form of the one dimensional VQHDM is presented in this section. The VQHDM given in Eqs. (7) and (8) is written as

$$\mathbf{W}_t + \mathbf{F}(\mathbf{W})_x = \left(\mathbf{B}\left(\mathbf{W};\mathbf{W}_x\right)\right)_x + \mathbf{S}(\mathbf{W}), \tag{10}$$

along with the following Poisson equation

$$\lambda^2 V_{xx} = n - C(x). \tag{11}$$

In Eq. (10), the left hand side shows a quasi-linear hyperbolic operator and the right hand side shows the diffusive terms. Also, **W**, **F**, **B** and **S** are the vector quantities which are defined as

$$\mathbf{W} = \begin{bmatrix} n \\ J \end{bmatrix},\ \mathbf{F}(\mathbf{W}) = \begin{bmatrix} J \\ \frac{J^2}{n} + Tn \end{bmatrix},$$

$$\mathbf{B}\left(\mathbf{W},\mathbf{W}_x\right) = \begin{bmatrix} \upsilon n_x \\ \upsilon J_x \end{bmatrix},\ \mathbf{S}(\mathbf{W}) = \begin{bmatrix} 0 \\ -J + n\left(\tilde{V} + Q\right)_x \end{bmatrix},$$

where, Q and $\tilde{V}$ are defined as $Q = \frac{\epsilon^2\partial_{xx}\sqrt{n}}{2\sqrt{n}}$ and $\tilde{V} = V + V_{ext}$ respectively. we assuming L for representing the length of typical device.

The initial conditions and boundary conditions are as under

$$n(x,0) = C(x), \qquad J(x,0) = 0. \tag{12}$$

$$n_x(0,t) = n_x(L,t) = 0, \qquad J_x(0,t) = J_x(L,t) = 0. \tag{13}$$

We considered the fixed-type boundary conditions for the density n due to the conservation of electron such as $n(L,t) = C(L)$ and $n(0,t) = C(0)$. Whereas, the boundary conditions for the potential V and applied voltage V_b in the Poisson equation are given in the form

$$V(L) = V_b, \quad V(0) = 0. \tag{14}$$

The multi-resolution WENO scheme for viscous quantum hydrodynamic model

This section includes the extension of FV MR-WENO scheme for solving the viscous quantum hydrodynamic model. First we consider the homogeneous form of the considered model given in Eq. (10) as follow

$$\mathbf{W}_t + \mathbf{F}(\mathbf{W})_x = \mathbf{0}, \quad t > 0, x \in \mathfrak{D} \tag{15}$$

and subdivide the domain $\mathfrak{D}$ into cells $C_i = [x_{i-\frac{1}{2}}, x_{i+\frac{1}{2}}]$ and $i = 1, \ldots, N$. The expression $x_i = \frac{1}{2}\left(x_{i-\frac{1}{2}} + x_{i+\frac{1}{2}}\right)$ represents the center of the i-th cell and $\triangle x_i$. represents the i-th cell size. Integrating Eq. (15) over the cell C_i yields

$$\frac{d}{dt}\overline{\mathbf{W}}(x_i,t) + \frac{1}{\triangle x_i}\left(\mathbf{F}(\mathbf{W}(x_{i+\frac{1}{2}},t)) - \mathbf{F}(\mathbf{W}(x_{i-\frac{1}{2}},t))\right) = \mathbf{0}, \tag{16}$$

where $\overline{\mathbf{W}}(x_i,t) = \frac{1}{\triangle x_i}\int_{x_{i-\frac{1}{2}}}^{x_{i+\frac{1}{2}}} \mathbf{W}(x,t)dx$. The Eq. (16) is approximated as

$$\frac{d}{dt}\overline{\mathbf{W}}_i(t) + \frac{1}{\triangle x_i}\left(\hat{\mathbf{F}}_{i+\frac{1}{2}} - \hat{\mathbf{F}}_{i-\frac{1}{2}}\right) = \mathbf{0}, \tag{17}$$

with monotone numerical flux $\hat{\mathbf{F}}_{i+\frac{1}{2}} = \mathcal{F}\left(\mathbf{W}^-_{i+\frac{1}{2}}, \mathbf{W}^+_{i+\frac{1}{2}}\right)$ and point-wise approximations to $\mathbf{W}(x_{i+\frac{1}{2}},t)$ are $\mathbf{W}^-_{i+\frac{1}{2}}$ and $\mathbf{W}^+_{i+\frac{1}{2}}$. Moreover, Lax-Friedrichs flux (LFF)is used as a monotone numerical flux given as

$$\mathcal{F}\left(\mathbf{W}^-_{i+\frac{1}{2}}, \mathbf{W}^+_{i+\frac{1}{2}}\right) = \frac{1}{2}\left(\mathbf{F}(\mathbf{W}^-_{i+\frac{1}{2}}) + \mathbf{F}(\mathbf{W}^+_{i+\frac{1}{2}}) - \vartheta(\mathbf{W}^+_{i+\frac{1}{2}} - \mathbf{W}^-_{i+\frac{1}{2}})\right), \tag{18}$$

where $\vartheta = \max_{\mathbf{W}}|\mathbf{F}'(\mathbf{W})|$. Now we compute the variables $\overline{\mathbf{W}}_i(t)$ which is used to approximate the cell average $\overline{\mathbf{W}}(x_i,t)$. The point-wise approximations $\mathbf{W}^-_{i+\frac{1}{2}}$ and $\mathbf{W}^+_{i+\frac{1}{2}}$ are calculated through the adjacent cell average values $\overline{\mathbf{W}}_i$ by WENO reconstruction. For the fifth order WENO reconstruction, we choose three central candidate stencils, $\mathbb{S}_1(i) = \{C_i\}$, $\mathbb{S}_2(i) = \{C_{i-1}, C_i, C_{i+1}\}$ and $\mathbb{S}_3(i) = \{C_{i-2}, C_{i-1}, C_i, C_{i+1}, C_{i+2}\}$ and reconstruct the zeroth, second and fourth degree polynomials $p_1(x), p_2(x)$ and $p_3(x)$ respectively, which satisfy

$$\frac{1}{\triangle x_i}\int_{x_{j-\frac{1}{2}}}^{x_{j+\frac{1}{2}}} p_1(x)dx = \overline{\mathbf{W}}_j, \ j = i, \tag{19}$$

$$\frac{1}{\triangle x_i}\int_{x_{j-\frac{1}{2}}}^{x_{j+\frac{1}{2}}} p_2(x)dx = \overline{\mathbf{W}}_j, \ j = i-1, i, i+1 \tag{20}$$

$$\frac{1}{\triangle x_i}\int_{x_{j-\frac{1}{2}}}^{x_{j+\frac{1}{2}}} p_3(x)dx = \overline{\mathbf{W}}_j, \ j = i-2, i-1, i, i+1, i+2. \tag{21}$$

More precisely, the explicit expressions for $p_1(x), p_2(x)$ and $p_3(x)$ are given as follow

$$p_1(x) = \overline{\mathbf{W}}_i,$$

$$p_2(x) = \frac{\overline{\mathbf{W}}_{i+1} - 2\overline{\mathbf{W}}_i + \overline{\mathbf{W}}_{i-1}}{2(\triangle x_i)^2}(x - x_i)^2 + \frac{\overline{\mathbf{W}}_{i+1} - \overline{\mathbf{W}}_{i-1}}{2(\triangle x_i)}(x - x_i) + \frac{-\overline{\mathbf{W}}_{i+1} + 26\overline{\mathbf{W}}_i - \overline{\mathbf{W}}_{i-1}}{24},$$

$$\begin{aligned} p_3(x) = \frac{1}{1920}\Bigg[& \frac{(80\overline{\mathbf{W}}_{i-2} - 320\overline{\mathbf{W}}_{i-1} + 480\overline{\mathbf{W}}_i - 320\overline{\mathbf{W}}_{i+1} + 80\overline{\mathbf{W}}_{i+2})}{(\triangle x_i)^4}(x - x_i)^4 \\ & + \frac{(160\overline{\mathbf{W}}_{i-2} - 320\overline{\mathbf{W}}_{i-1} + 320\overline{\mathbf{W}}_{i+1} - 160\overline{\mathbf{W}}_{i+2})}{(\triangle x_i)^3}(x - x_i)^3 \\ & + \frac{(120\overline{\mathbf{W}}_{i-2} - 1440\overline{\mathbf{W}}_{i-1} + 2640\overline{\mathbf{W}}_i - 1440\overline{\mathbf{W}}_{i+1} + 120\overline{\mathbf{W}}_{i+2})}{(\triangle x_i)^2}(x - x_i)^2 \\ & + \frac{(200\overline{\mathbf{W}}_{i-2} - 1360\overline{\mathbf{W}}_{i-1} + 1360\overline{\mathbf{W}}_{i+1} - 200\overline{\mathbf{W}}_{i+2})}{(\triangle x_i)}(x - x_i) \\ & + (9\overline{\mathbf{W}}_{i-2} - 116\overline{\mathbf{W}}_{i-1} + 2134\overline{\mathbf{W}}_i - 116\overline{\mathbf{W}}_{i+1} + 9\overline{\mathbf{W}}_{i+2})\Bigg]. \end{aligned}$$

The point-wise reconstructed values $\mathbf{W}^+_{i+\frac{1}{2}}$ and $\mathbf{W}^-_{i+\frac{1}{2}}$ are obtained by the following relations

$$\mathbf{W}^+_{i+\frac{1}{2}} = \omega_1\hat{\mathbf{W}}^1_{i+\frac{1}{2}} + \omega_2\hat{\mathbf{W}}^2_{i+\frac{1}{2}} + \omega_3\hat{\mathbf{W}}^3_{i+\frac{1}{2}}, \tag{22}$$

$$\mathbf{W}^-_{i+\frac{1}{2}} = \tilde{\omega}_1\tilde{\mathbf{W}}^1_{i-\frac{1}{2}} + \tilde{\omega}_2\tilde{\mathbf{W}}^2_{i-\frac{1}{2}} + \tilde{\omega}_2\tilde{\mathbf{W}}^2_{i-\frac{1}{2}}, \tag{23}$$

where $\hat{\mathbf{W}}^l_{i+\frac{1}{2}}$ and $\tilde{\mathbf{W}}^l_{i-\frac{1}{2}}$, for $l = 1, 2, 3$, are reconstructed values and defined as

$$\hat{\mathbf{W}}^1_{i+\frac{1}{2}} = p_1(x_{i+\frac{1}{2}}), \tag{24}$$

$$\hat{\mathbf{W}}^2_{i+\frac{1}{2}} = \frac{1}{\xi_{2,2}}p_2(x_{i+\frac{1}{2}}) - \frac{\xi_{1,2}}{\xi_{2,2}}\hat{\mathbf{W}}^1_{i+\frac{1}{2}}, \tag{25}$$

$$\hat{\mathbf{W}}^3_{i+\frac{1}{2}} = \frac{1}{\xi_{3,3}}p_3(x_{i+\frac{1}{2}}) - \frac{\xi_{1,3}}{\xi_{3,3}}\hat{\mathbf{W}}^1_{i+\frac{1}{2}} - \frac{\xi_{2,3}}{\xi_{3,3}}\hat{\mathbf{W}}^2_{i+\frac{1}{2}}, \tag{26}$$

with

$$p_1(x_{i+\frac{1}{2}}) = \overline{\mathbf{W}}_i, \tag{27}$$

$$p_2(x_{i+\frac{1}{2}}) = \frac{-1}{6}\overline{\mathbf{W}}_{i-1} + \frac{5}{6}\overline{\mathbf{W}}_i + \frac{1}{3}\overline{\mathbf{W}}_{i+1}, \tag{28}$$

$$p_3(x_{i+\frac{1}{2}}) = \frac{1}{30}\overline{\mathbf{W}}_{i-2} - \frac{13}{60}\overline{\mathbf{W}}_{i-1} + \frac{47}{60}\overline{\mathbf{W}}_i + \frac{9}{20}\overline{\mathbf{W}}_{i+1} + \frac{1}{20}\overline{\mathbf{W}}_{i+2}. \tag{29}$$

Where $\xi_{1,2} + \xi_{2,2} = 1$, $\xi_{1,3} + \xi_{2,3} + \xi_{3,3} = 1$ and $\xi_{2,2}, \xi_{3,3} \neq 0$. In these expressions, $\xi_{1,2}, \xi_{2,2}$ are the linear weights. For a balance between the sharp and essentially non-oscillatory shock transitions in non-smooth regions and accuracy in smooth regions, we set the linear weights as $\xi_{1,2} = 1/11$, $\xi_{2,2} = 10/11$, $\xi_{1,3} = 1/111$, $\xi_{2,3} = 10/111$ and $\xi_{3,3} = 100/111$ for the fifth order approximation, as described in [22].

The non linear weights ω_l in Eq. (22) are defined as The non linear weights are then given as

$$\omega_l = \frac{\bar{\omega}_l}{\sum_{l=1}^m \bar{\omega}_l}, \quad \bar{\omega}_l = \xi_{l,m}\left(1 + \frac{\tau}{\epsilon + \mathfrak{B}_l}\right), \ l = 1, \ldots, m; \ \ m = 3. \tag{30}$$

Here ϵ is taken as 10^{-10} in all the simulations. Here, ξ_l and $\mathfrak{B}_l$ respectively denote the linear weights and smoothness indicators. These smoothness indicators in general form is written as

$$\mathfrak{B}_m = \sum_{j=1}^{k}\int_{x_{i-\frac{1}{2}}}^{x_{i+\frac{1}{2}}} h^{2j-1}\left(\frac{d^j p_m(x)}{dx^j}\right)^2 dx, \quad m = 2, 3, \tag{31}$$

where $k = 2(m-1)$ for $m = 2, 3$, respectively. Here, the values of $\mathfrak{B}_1, \mathfrak{B}_2$ and $\mathfrak{B}_3$ are defined in the same way as described in [22,32,33]. More precisely, these smooth indicators are defined as follow

$$\mathfrak{B}_2 = \frac{13}{12}\left(\overline{\mathbf{W}}_{i-1} - 2\overline{\mathbf{W}}_i + \overline{\mathbf{W}}_{i+1}\right)^2 + \frac{1}{4}\left(\overline{\mathbf{W}}_{i-1} - \overline{\mathbf{W}}_{i+1}\right)^2, \tag{32}$$

Table 1
L^1-error and numerical order of accuracy for $U = 0$ in Test problem 1.

No of cells	n	
	L^1-error	Order
100	0.97	–
200	0.041	4.56
400	0.0015	4.77
800	0.00006	4.644
1600	0.0000021	4.8365

$$\mathfrak{B}_3 = \left(\eta_1 + \frac{1}{10}\eta_3\right)^2 + \frac{13}{3}\left(\eta_2 + \frac{123}{455}\eta_4\right)^2 + \frac{781}{20}(\eta_3)^2 + \frac{1421461}{2275}(\eta_4), \tag{33}$$

where

$$\eta_1 = \frac{1}{120}\left(11\overline{\mathbf{W}}_{i-2} - 82\overline{\mathbf{W}}_{i-1} + 82\overline{\mathbf{W}}_{i+1} - 11\overline{\mathbf{W}}_{i+2}\right), \tag{34}$$

$$\eta_2 = \frac{1}{56}\left(-3\overline{\mathbf{W}}_{i-2} + 40\overline{\mathbf{W}}_{i-1} - 74\overline{\mathbf{W}}_{i+1} + 40\overline{\mathbf{W}}_{i+1} - 3\overline{\mathbf{W}}_{i+2}\right), \tag{35}$$

$$\eta_3 = \frac{1}{12}\left(-\overline{\mathbf{W}}_{i-2} + 2\overline{\mathbf{W}}_{i-1} - 2\overline{\mathbf{W}}_{i+1} + \overline{\mathbf{W}}_{i+2}\right), \tag{36}$$

$$\eta_4 = \frac{1}{24}\left(\overline{\mathbf{W}}_{i-2} - 4\overline{\mathbf{W}}_{i-1} + 6\overline{\mathbf{W}}_{i} - 4\overline{\mathbf{W}}_{i+1} + \overline{\mathbf{W}}_{i+2}\right). \tag{37}$$

Now for resolving the discontinuities efficiently, the expression of $\mathfrak{B}_1$ is defined as follow

$$\delta_0 = \left(\overline{\mathbf{W}}_i - \overline{\mathbf{W}}_{i-1}\right)^2, \quad \delta_1 = \left(\overline{\mathbf{W}}_{i+1} - \overline{\mathbf{W}}_i,\right)^2 \tag{38}$$

$$\bar{\xi}_{0,1} = \begin{cases} 1, & \delta_0 > \delta_1, \\ 10, & otherwise \end{cases}, \quad \bar{\xi}_{1,1} = 1 - \bar{\xi}_{0,1}, \tag{39}$$

$$\xi_{0,1} = \frac{\bar{\xi}_{0,1}}{\bar{\xi}_{0,1} + \bar{\xi}_{1,1}}, \qquad \xi_{1,1} = 1 - \xi_{0,1}, \tag{40}$$

$$\sigma_0 = \xi_{0,1}\left(1 + \frac{|\delta_0 - \delta_1|^2}{\delta_0 + \varepsilon}\right), \quad \sigma_1 = \xi_{1,1}\left(1 + \frac{|\delta_0 - \delta_1|^2}{\delta_1 + \varepsilon}\right), \quad \sigma = \sigma_0 + \sigma_1. \tag{41}$$

In Eq. (41), ε is a small positive number to avoid the denominator to become zero. Finally we set

$$\mathfrak{B}_1 = \frac{1}{\sigma^2}\left(\sigma_0(\overline{\mathbf{W}}_i - \overline{\mathbf{W}}_{i-1}) + \sigma_1(\overline{\mathbf{W}}_{i+1} - \overline{\mathbf{W}}_i)\right). \tag{42}$$

The term τ in Eq. (30) is given as

$$\tau = \left(\frac{\sum_{l=1}^{2}|\mathfrak{B}_3 - \mathfrak{B}_l|}{2}\right). \tag{43}$$

This completes the spatial reconstruction procedure.

Next, we discretize the right hand side of (10). We denote the $\mathbf{B}_i$ and $\mathbf{S}_i$ are approximations of the $\int_{x_{i-\frac{1}{2}}}^{x_{i+\frac{1}{2}}}\left(\mathbf{B}\left(U;U_x\right)\right)_x dx$ and $\int_{x_{i-\frac{1}{2}}}^{x_{i+\frac{1}{2}}}\mathbf{S}(U)dx$ respectively and defined as follow

$$\mathbf{B}_i = \left(\nu\frac{n_{i-1} - 2n_i + n_{i+1}}{(\triangle x_i)^2}, \nu\frac{j_{i-1} - 2j_i + j_{i+1}}{(\triangle x_i)^2}\right)^T, \tag{44}$$

and

$$\mathbf{S}_i = \left(0, (-j_i) + (\frac{n_i}{2\triangle x_i})(\tilde{V}_{i+1} - \tilde{V}_{i-1} + \tilde{Q}_{i+1} - \tilde{Q}_{i-1})\right)^T, \tag{45}$$

where T denotes the transpose. Next, the Poisson Eq. (11) is discretized as follow

$$\lambda^2\left(\frac{V_{i+1} - 2V_i + V_{i-1}}{(\triangle x_i)^2}\right) = n_i - C(x_i), \quad i = 1, \ldots, N-1 \tag{46}$$

and obtain the potential V_i at the nth time level, by using the boundary conditions that are described in Eq. (14). Finally, we end up with the semi-discrete equation as follow

$$\frac{d}{dt}\overline{\mathbf{W}}_i(t) = -\frac{1}{\triangle x_i}\left(\hat{\mathbf{F}}_{i+\frac{1}{2}} - \hat{\mathbf{F}}_{i-\frac{1}{2}}\right) + \frac{1}{\triangle x_i}\left(\mathbf{B}_i + \mathbf{S}_i\right), \tag{47}$$

or the above equation can be written as

$$\frac{d}{dt}\overline{\mathbf{W}}_i(t) = \mathcal{L}(\mathbf{W}). \tag{48}$$

Now, for solving the system of ordinary differential eq. (48), we apply the third order TVD RK method [22] as follow

$$\begin{aligned} \mathbf{W}^{(1)} &= \mathbf{W}^n + dt\mathcal{L}(\mathrm{u}^n), \\ \mathbf{W}^{(2)} &= \frac{3}{4}\mathbf{W}^n + \frac{1}{4}\left(\mathbf{W}^{(1)} + dt\mathcal{L}(\mathbf{W}^{(1)})\right), \\ \mathbf{W}^{(n+1)} &= \frac{1}{3}\mathbf{W}^n + \frac{2}{3}\left(\mathbf{W}^{(2)} + dt\mathcal{L}(\mathbf{W}^{(2)})\right), \end{aligned} \tag{49}$$

where $\mathcal{L}(\mathrm{u})$ is the spatial operator.

Numerical test problems

In this section, the performance and accuracy of the proposed scheme is checked by taking various test problems. Further, the kinetic flux vector splitting numerical scheme is used to compare the results those obtained by proposed numerical scheme.

Test problem 1: First we investigate the effect of viscous and quantum terms on a ballistic $n^+ - n - n^+$ diode. Here we consider same initial data as taken in [14], for checking the efficiency of proposed numerical scheme. The doping profile is taken as

$$C(x) = 1 + 0.45(\tanh(1000x - 600) - \tanh(1000x - 400)), \ 0 \le x \le 1, \tag{50}$$

and scaled parameters are taken as follow

$$\nu = 4.267 \times 10^{-3}, \ \epsilon = 0.00289, \ \lambda = 0.1 \text{ and } \tau = 0.125.$$

The solution profiles of density of electron for different scaled applied voltages are given in Fig. 1. These different values are $(i)\mathrm{U} = 0, (ii)\mathrm{U} = 4, (iii)\mathrm{U} = 5, (iv)\mathrm{U} = 6$. The oscillations in solution profiles for the values of applied voltages U = 5 and U = 6 as shown in Fig. 1 are not a numerical artifact. These oscillations are produced by the quantum term, for more detail see [14]. The results obtained by KFVS scheme and proposed scheme are compared with each other. From Fig. 1, clearly, there is a good agreement between both schemes but KFVS numerical scheme is more diffusive as compare to MR-WENO scheme.

Further, the order of numerical accuracy is calculated for the values of applied voltage $U = 0$. The reference solution is calculated at 10,000 grid cells and treated as the exact solution. The L^1-error and order of numerical accuracy for the MR-WENO scheme are given in Table 1.

Test problem 2: Different Doping:

In this test problem, we considered $C^* = 10^{24}$ m^3 for measuring doping in m^3. We also considered a semiconductor whose length is $L = 125$ nm. The device consists of three regions that is (i) drain region (ii) channel and (iii) source. The length of drain region is [75 nm, 125 nm] and the length of source is [0 nm, 50 nm] whereas the length of channel region is [50 nm, 75 nm]. The following values are used for scaled parameters such as $\lambda^2 = 3.032\times10^{-4}$, $\epsilon^2 = 3.893\times10^{-3}$, $T = 1.00585$ and $\upsilon = 9.935 \times 10 - 4$. A doping density profile for this test problem is as under

$$C(x) = [1.0 + 0.4599(\tanh(10x - 750) - \tanh(10x - 750))] \times 10^{24}, \quad x \in [0 \text{ nm}, 125 \text{ nm}] \tag{51}$$

V_{ext} is defined below

$$V_{ext} = \begin{cases} 0.209V, & x \in (50 \text{ nm}, 75 \text{ nm}), \\ 0, & elsewhere. \end{cases} \tag{52}$$

The length of GaAs diode is to be considered as $L = 125$ nm which is kept at $T_0 = 77$ K and applied voltage is $V_b = 1.5V$. Fig. 2 shows the numerical results on 200 grid points for physical variables. We can observe the behavior of electron density which is steady state in both source as well as drain region as shown in Fig. 2. we can see the perturbation in channel by applying applied voltage and external

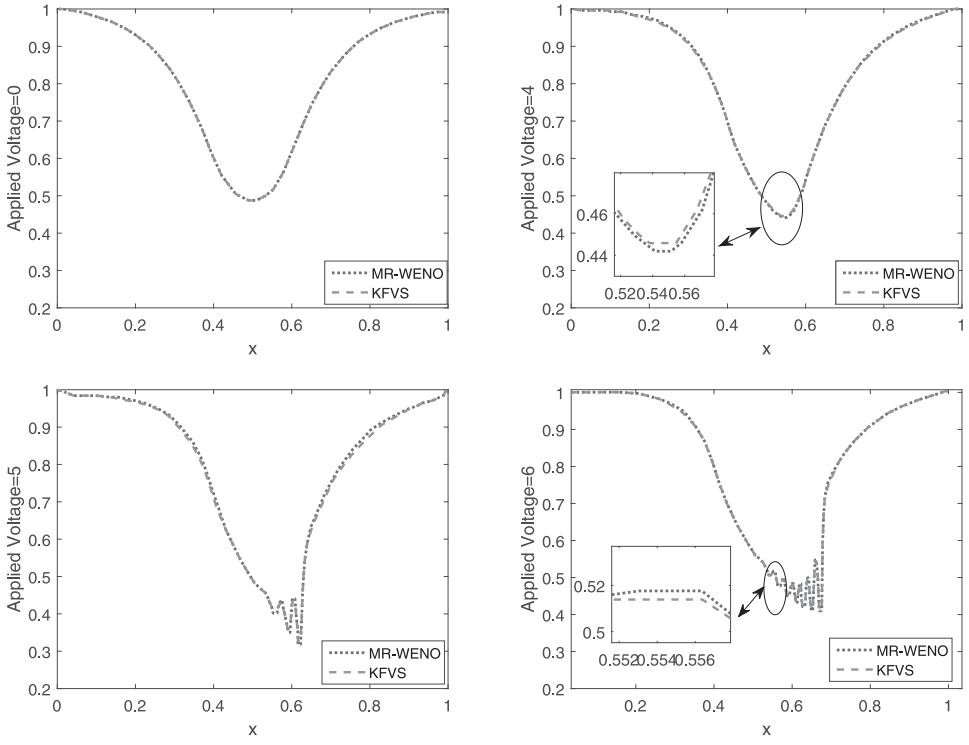

Fig. 1. Solution profiles are computed by MR-WENO and KFVS numerical schemes.

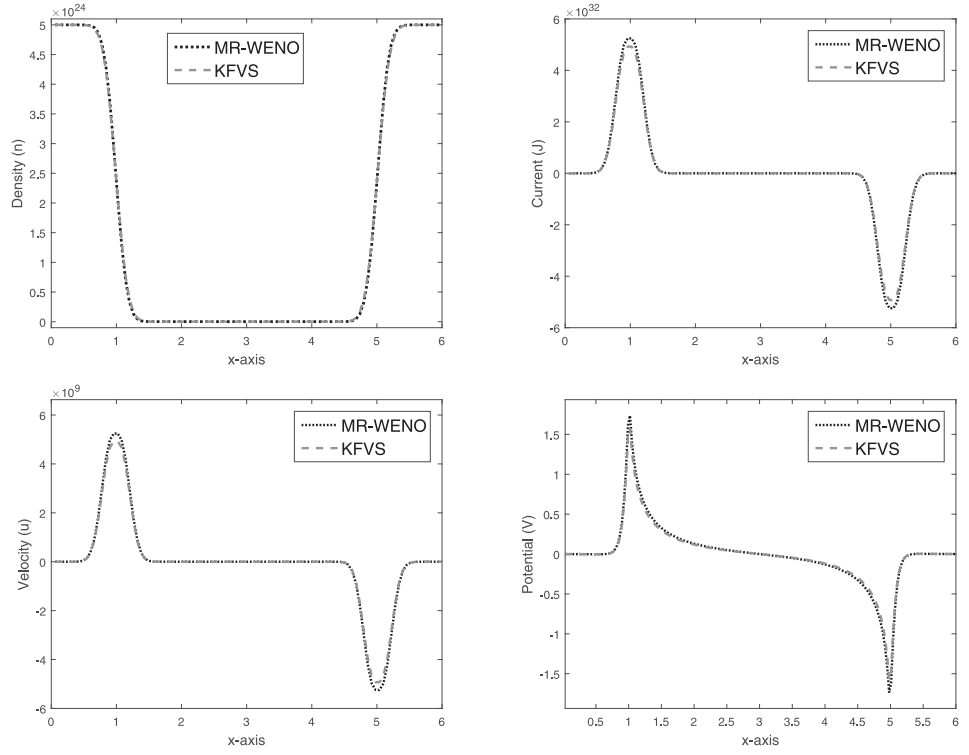

Fig. 2. Solution profiles are computed by MR-WENO and KFVS numerical schemes.

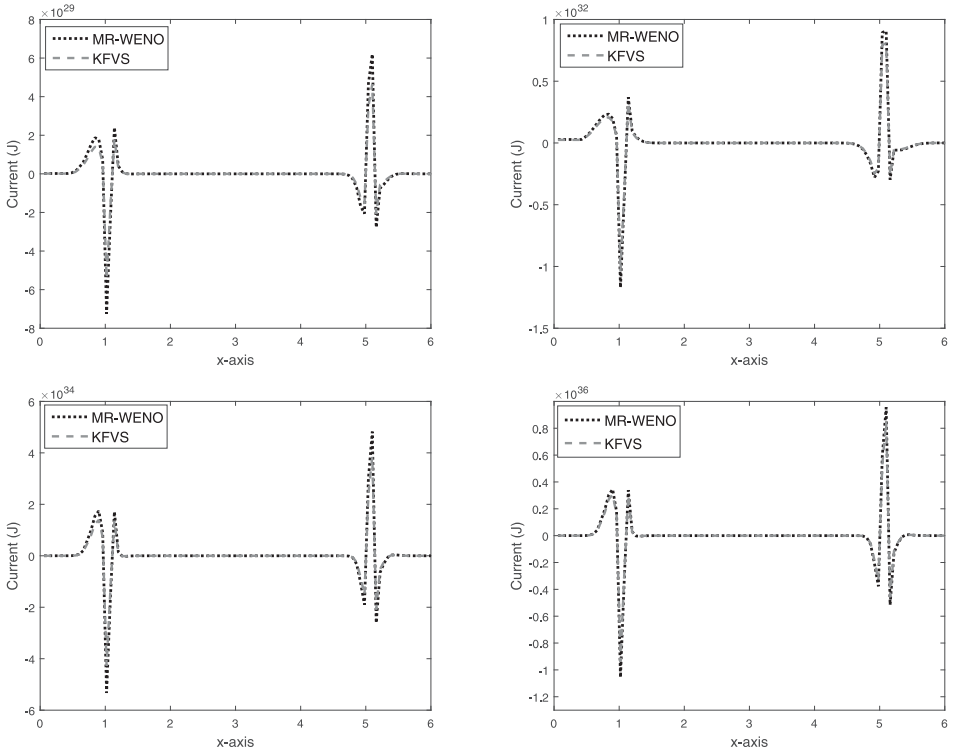

Fig. 3. Solution profiles are computed by MR-WENO and KFVS numerical schemes.

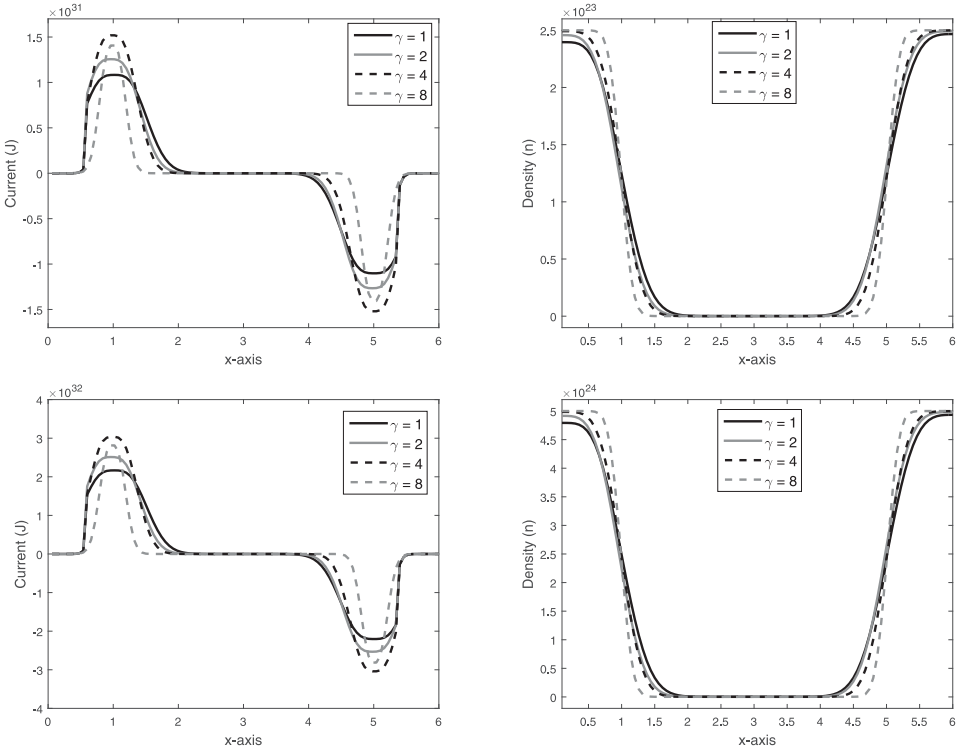

Fig. 4. The top two Solution profiles are computed by KFVS and bottom two are solution profiles are computed by MR-WENO.

potential V_{ext}. Similarly, velocity, current and potential profiles show the same pattern. The numerical results obtained by MR-WENO scheme and KFVS schemes are compared with each other. The MR-WENO scheme shows better performance while capturing peaks and resolving the sharp discontinuities.

Test problem 3: Different external potential V_{ext}

The length of GaAs diode is to be considered as $L = 0.6$ μm which is kept at $T_0 = 77$ K and applied voltage is $V_b = 0.8V$. The doping density profile is same as in Test problem 2. In this problem, we checked the effect of external potential at its different values on current density solution profiles, as shown in Fig. 3. The different values of external potential $V_{ext} = -2.09 \times 10^{-1}V$ and $V_{ext} = -2.09 \times 10^{-2}V$ for $x \in (0.1\ \mu m, 0.4\ \mu m)$ are used in the first row of Fig. 3 and similarly $V_{ext} = -2.09 \times 10^{-3}V$ and $V_{ext} = -2.09 \times 10^{-4}V$ for $x \in (0.1\ \mu m, 0.4\ \mu m)$ are used in the last row of Fig. 3. The Fig. 3 shows that the current flow in device increases when external potential is decreasing, such types of results are showed in [21]. Again both schemes behave very well but MR-WENO scheme captures the peaks more efficiently.

Test problem 4: The effect of different viscosities

In this test problem, we will analyzed the physical parameters such as viscosity. Here, once again we will simulate the Test problem 2 for viscosity $\upsilon = \upsilon_0/\gamma$ at different values of γ such as $\gamma = 1, 2, 4, 8$. The solutions of particle densities obtained from MR-WENO and KFVS numerical schemes at different values of viscosity are shown in Fig. 4. We observe that there is a smooth transition at large value of viscosity. In other words, particles move from left side to right around the junction and then they enter into the supersonic region at $x = 1$. However, the solution obtained from inviscid [14] and viscous model are same at small value of viscosity *i.e* $\upsilon = \frac{1}{8}\upsilon_0 \approx 5.0 \times 10^{-5}$.

Conclusions

Multi-resolution finite volume WENO scheme was developed to investigate the non linear viscous quantum hydrodynamical model for the semiconductor devices. Despite the non linear transport phenomenon, sharp gradients and source terms in the considered model, the proposed numerical scheme captured the peaks efficiently and suppressed the unwanted oscillations near the steep gradients. The accuracy and robustness of proposed numerical scheme was checked by considering the different test problems. Moreover, the results obtained by using the considered scheme were compared with the results those obtained by the KFVS numerical scheme. This comparison found the good agreement between the both numerical schemes but KFVS numerical scheme was more diffusive as compare to the MR-WENO scheme.

Declaration of competing interest

The authors declare that they have no known competing financial interests or personal relationships that could have appeared to influence the work reported in this paper.

References

[1] Ancona MG, Iafrate GI. Quantum correction to the equation of state of an electron gas in a semiconductor. Phys Rev B 1989;39:9536–40.

[2] Zhou J, Ferry DK. Simulation of ultra-small GaAs MESFET using quantum moment equations. IEEE Trans Electron Devices 1992;39:473–8.

[3] Wettstein A. Quantum e registered ects in MOS devices. In: Series in microelectronics, vol. 94. Konstanz: Hartung-Gorre; 2000.

[4] Degond P, Ringhofer C. Quantum moment hydrodynamics and the entropy principle. J Stat Phys 2003;112:587–628.

[5] Gardner CL. The quantum hydrodynamic model for semiconductor devices. SIAM J Appl Math 1994;54:409–27.

[6] Markowich PA, Ringhofer CA, Schmeiser C. Semiconductor equations. Berlin: Springer; 1990.

[7] Jungel A. Quasi-hydrodynamic semiconductor equations. In: Progress in nonlinear differential equations. Basel: Birkhauser; 2001.

[8] Buot F, Jensen K. Lattice WeylWigner formulation of exact many-body quantum-transport theory and applications to novel solid-state quantum-based devices. Phys Rev B 1990;42:9429–57.

[9] Argyres P. Quantum kinetic equations for electrons in high electric and phonon fields. Phys Lett A 1992;171:373–9.

[10] Eu B, Mao CK. Quantum kinetic theory of irreversible thermodynamics: Low-density gases. Phys Rev E 1994;50:4380–98.

[11] Frommlet F, Markowich P, Ringhofer C. A Wigner function approach to phonon scattering. VLSI Des 1999;9:339–50.

[12] Lui Y, Shu W. Local discontinuous Galerkin methods for moment models in device simulations: Performance assessment and two-dimensional results. Appl Numer Math 2007;57:629–45.

[13] Hoseinzadeh S, et al. J Mater Sci, Mater Electron 2017;28:14855. http://dx.doi.org/10.1007/s10854-017-7357-9.

[14] Jungel A, Tang S. Numerical approximation of the viscous quantum hydrodynamic model for semiconductors. Appl Numer Math 2006;1:19–46.

[15] Gualdani MP, Jüngel A. Analysis of the viscous quantum hydrodynamic equations for semiconductors. European J Appl Math 2004;15(5):577.

[16] Gualdani M, Jungel A, Toscani G. Exponential decay in time of solutions of the viscous quantum hydrodynamic equations. J Appl Math 2003;16:1273–8.

[17] Jungel A, Milisic J. Physical and numerical viscosity for quantum hydrodynamics. Comm Math Phys 2007;5:447–71.

[18] Chen L, Dreher M. The viscous model of quantum hydrodynamics in several dimensions. Math Models Methods Appl Sci 2007;17:1065–93.

[19] Dreher M. The transient equations of viscous quantum hydrodynamics. Math Models Methods Appl Sci 2008;31:391–414.

[20] Gamba IM, Jungel A, Vasseur A. Global existence of solutions to one-dimensional viscous quantum hydrodynamic equations. J Differ Equ 2009;247:3117–35.

[21] Nisar UA, Ashraf W, Qamar S. Application of kinetic flux vector splitting scheme for solving viscous quantum hydrodynamical model of semiconductor devices. Res Phys 2018;11:629–37.

[22] Zhu J, Shu C-W. A new type of multi-resolution WENO schemes with increasingly higher order of accuracy. J Comput Phys 2018;375:659–83.

[23] Liu XD, Osher S, Chan T. Weighted essentially non-oscillatory schemes. J Comput Phys 1994;115:200–12.

[24] Jiang G, Shu C-W. Efficient implementation of weighted ENO schemes. J Comput Phys 1996;126:202–28.

[25] Harten A. Multi-resolution analysis for ENO schemes. Contract No. NAS1-18605, Institute for Computer Applications in Science and Engineering, NASA Langley Research Center; 1991, p. 23665–5225.

[26] Dahmen W, Gottschlich-Mller S. Multiresolution schemes for conservation laws. Numer Math 2001;88:399–443.

[27] Gasser I, et al. Macroscopic theory of charged quantum fluids. In: Marcati P, editor. Mathematical problems in semiconductor physics. 1995. p. 42-75.

[28] Petruccioli S. Correspondence principle versus Planck-type theory of the atom. Arch Hist Exact Sci 2014;68:599–639.

[29] Caldeira A, Leggett A. Path integral approach to quantum brownian motion. Phys A 1983;121:587–616.

[30] Arnold A, et al. An analysis of Quantu Fokker-Planck models: A Wigner function approach. Germany: TU Berlin; 2000, Preprint.

[31] Castella F, Erdos L, Frommlet F, Markowich P. Fokker-Planck equations as scaling limits of reversible quantum systems. J Stat Phys 2000;100:543–601.

[32] Shu C-W. High-order finite difference and finite volume WENO schemes and discontinuous Galerkin methods for CFD. Int J Comput Fluid Dyn 2003;30:107–18.

[33] Shu C-W. High order weighted essentially nonoscillatory schemes for convection dominated problems. SIAM Rev 2009;51:82–126.